Article

Cell Reports

# Mammalian Reverse Genetics without Crossing Reveals *Nr3a* as a Short-Sleeper Gene

## Graphical Abstract

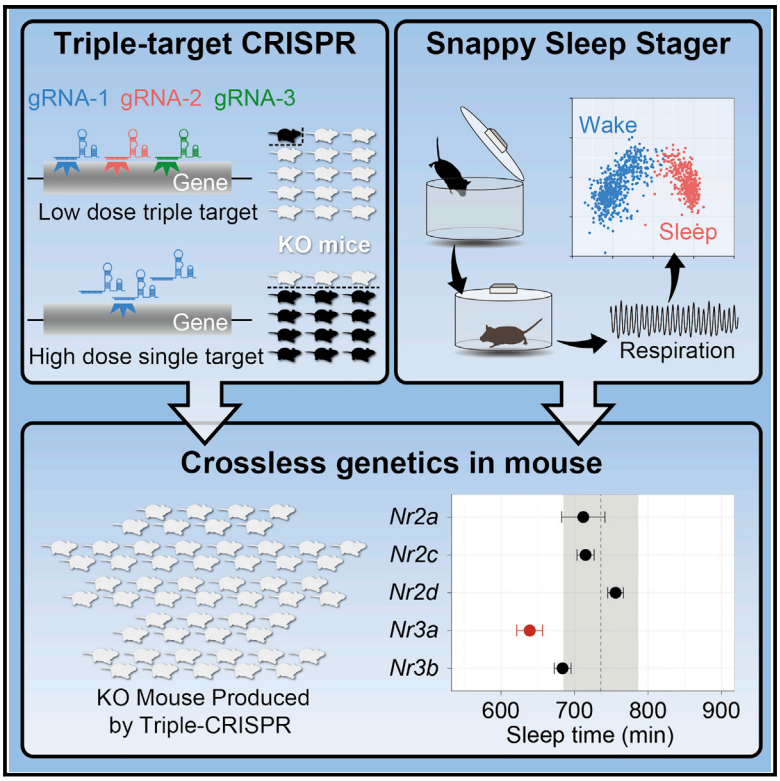


## Highlights

- A triple-target CRISPR method achieved almost perfect knockout efficiency
- SSS achieved non-invasive fully automated high-performance sleep phenotyping
- Genetics without crossing revealed *Nr3a* as a short-sleeper gene

## Authors

Genshiro A. Sunagawa, Kenta Sumiyama, Maki Ukai-Tadenuma, Dimitri Perrin, ..., Koji L. Ode, Shigehiro Kuraku, Hiroki R. Ueda

## Correspondence

uedah-tky@umin.ac.jp

## In Brief

Sunagawa et al. present an application of mammalian reverse genetics without crossing by developing two methods. The authors improve KO mice production using a triple-target CRISPR and combine this with a non-invasive respiration-based automated sleep phenotyping system, the Snappy Sleep Stager. Combining these methods, the authors found that the *Nr3a* KO is a short-sleeper.

Sunagawa et al., 2016, Cell Reports *14*, 1–16
January 26, 2016 
http://dx.doi.org/10.1016/j.celrep.2015.12.052

CellPress

Please cite this article in press as: Sunagawa et al., Mammalian Reverse Genetics without Crossing Reveals *Nr3a* as a Short-Sleeper Gene, Cell Reports (2016), http://dx.doi.org/10.1016/j.celrep.2015.12.052

Cell Reports
Article



# Mammalian Reverse Genetics without Crossing Reveals *Nr3a* as a Short-Sleeper Gene

Genshiro A. Sunagawa,[1,8] Kenta Sumiyama,[2,8] Maki Ukai-Tadenuma,[1,8] Dimitri Perrin,[1,6,8] Hiroshi Fujishima,[1] Hideki Ukai,[1] Osamu Nishimura,[5] Shoi Shi,[3] Rei-ichiro Ohno,[3] Ryohei Narumi,[1] Yoshihiro Shimizu,[7] Daisuke Tone,[3] Koji L. Ode,[3] Shigehiro Kuraku,[5] and Hiroki R. Ueda[1,3,4,*]

[1]Laboratory for Synthetic Biology, RIKEN Quantitative Biology Center, 1-3 Yamadaoka, Suita, Osaka 565-0871, Japan
[2]Laboratory for Mouse Genetic Engineering, RIKEN Quantitative Biology Center, 1-3 Yamadaoka, Suita, Osaka 565-0871, Japan
[3]Department of Systems Pharmacology, Graduate School of Medicine, The University of Tokyo, 7-3-1 Hongo, Bunkyo-ku, Tokyo 113-0033, Japan
[4]CREST, Japan Science and Technology Agency, 4-1-8 Honcho, Kawaguchi, Saitama 332-0012, Japan
[5]Phyloinformatics Unit, RIKEN Center for Life Science Technologies, 2-2-3 Minatojima-minamimachi, Chuo-ku, Kobe, Hyogo 650-0047, Japan
[6]School of Electrical Engineering and Computer Science, Science and Engineering Faculty, Queensland University of Technology, GPO Box 2434, Brisbane, QLD 4001, Australia
[7]Laboratory for Cell-Free Protein Synthesis, RIKEN Quantitative Biology Center, 6-2-3, Furuedai, Suita, Osaka 565-0874, Japan
[8]Co-first author
*Correspondence: uedah-tky@umin.ac.jp
http://dx.doi.org/10.1016/j.celrep.2015.12.052


## SUMMARY

**The identification of molecular networks at the system level in mammals is accelerated by next-generation mammalian genetics without crossing, which requires both the efficient production of whole-body biallelic knockout (KO) mice in a single generation and high-performance phenotype analyses. Here, we show that the triple targeting of a single gene using the CRISPR/Cas9 system achieves almost perfect KO efficiency (96%–100%). In addition, we developed a respiration-based fully automated non-invasive sleep phenotyping system, the Snappy Sleep Stager (SSS), for high-performance (95.3% accuracy) sleep/wake staging. Using the triple-target CRISPR and SSS in tandem, we reliably obtained sleep/wake phenotypes, even in double-KO mice. By using this system to comprehensively analyze all of the *N*-methyl-*D*-aspartate (NMDA) receptor family members, we found *Nr3a* as a short-sleeper gene, which is verified by an independent set of triple-target CRISPR. These results demonstrate the application of mammalian reverse genetics without crossing to organism-level systems biology in sleep research.**

## INTRODUCTION

The system-level identification of molecular networks in organisms is an important challenge in biology (Kitano, 2002a, 2002b). Classical reverse genetics requires several generations of animal crosses to produce mutant animals of sufficient quality and quantity for phenotype analysis. Conventional methods for producing knockout (KO) mice usually involve targeting-vector construction (~2 weeks), the introduction of target mutations into embryonic stem cells (ESCs) by homologous recombination (a few weeks), and the injection of the mutant ESCs into wild-type blastocysts to produce chimera mice (~3 weeks). If the mutant ESCs contribute to the germline of the newborn chimera mice, their next-generation offspring will possess a heterozygous mutation (~3 months). Further crossings of the offspring (several months to years; at least 3 months per generation) will produce mice with completely homozygous KO mutations on an inbred genomic background, which is required for reliable phenotype analysis. Thus, conventional methods require substantial amounts of time, space, and effort to knock out even a single gene (Nagy, 2003). Therefore, identification of molecular networks comprehensively in organisms will require "next-generation" genetics, i.e., genetic alterations without crossing. Toward this goal, both highly efficient (>90%) mutant production in a single generation and highly accurate (>90%) phenotype analyses of mutant animals are needed.

The efficient production of biallelic KO mice can be facilitated by recently developed genome editing techniques, including ZFNs (zinc-finger nucleases) (Carbery et al., 2010), TALENs (transcription-activator-like effector nucleases) (Sung et al., 2013), and the CRISPR/Cas nuclease systems (Hsu et al., 2014; Wang et al., 2013). Unlike the protein-based ZFNs and TALENs, the CRISPR/Cas system uses RNA-based DNA recognition derived from a bacterial adaptive immune system (Horvath and Barrangou, 2010; Wiedenheft et al., 2012). This method accelerates the generation of KO animals via the co-injection of RNA encoding the Cas9 protein and target-locus-specific guide RNAs (gRNAs) into embryos (Fujii et al., 2013; Wang et al., 2013). Several modifications of the CRISPR/Cas9 system have been also introduced to improve the efficiency and specificity of targeted mutations in a genome (Fu et al., 2014; Ran et al., 2013; Zhou et al., 2014). However, two problems remain: (1) first-generation mice often contain a mosaic of wild-type and KO cells, and

Please cite this article in press as: Sunagawa et al., Mammalian Reverse Genetics without Crossing Reveals *Nr3a* as a Short-Sleeper Gene, Cell Reports (2016), http://dx.doi.org/10.1016/j.celrep.2015.12.052

(2) the rate of complete biallelic mutant mice generated is relatively low (usually ~60%–80% at best). Therefore, the highly efficient (>90%) production of whole-body biallelic KO in a single generation remains a fundamental challenge for organism-level systems biology.

The comprehensive identification of molecular circuits at the organism level also requires accurate (>90%) phenotype analysis. In neuroscience, sleep/wake behavior is an intriguing phenotype, because sleep disorders (e.g., insomnia or hypersomnia) are sensitive and informative symptoms of almost all psychological disorders. Sleep/wake states have been characterized in humans by electroencephalography (EEG) and electromyography (EMG). For example, during sleep, EEG mostly displays high-amplitude, low-frequency fluctuations, whereas during waking, it exhibits low-amplitude, high-frequency fluctuations. On the other hand, EMG displays low-amplitude fluctuations during sleep and high-amplitude fluctuations during waking. These characteristic EEG/EMG patterns during sleep and waking are preserved in mammals and can be measured by electrodes surgically implanted in the brain and muscles. However, such recording requires special surgical skills, and the surgery is highly invasive, requiring a long recovery period (more than 10 days) after implantation before sleep/wake recording. Furthermore, the EEG/EMG data are often manually annotated and classified into sleep/wake phenotypes by visual assessment, which can be time consuming and somewhat subjective. Therefore, sleep/wake phenotyping has been a low-throughput method; for comprehensive studies, a scalable, non-invasive, fully automated sleep/wake recording method is needed.

In this study, we developed a simple theory to predict the minimum efficacy of different CRISPR methods for the highly efficient production of whole-body biallelic KO mice. As we predicted, triple-target CRISPR elicited almost perfect (~96%–100%) whole-body KO of the *Tyrosinase* (*Tyr*) gene, which is functionally evaluated by animal coat color. This KO efficiency was confirmed using three independent sets of gRNAs. The highly efficient production of whole-body KO by the triple-target CRISPR method also enabled us to obtain clock mutant phenotypes reliably, not only of *Bmal1* single-KO mice but also of *Cry1*/*Cry2* or *Per1*/*Per2* double-KO mice. For accurate phenotype analysis, we developed a respiration-based, non-invasive, fully automated system, the Snappy Sleep Stager (SSS), which enabled the high-performance analysis (95.3% accuracy) of sleep/wake phenotypes. Using the triple-target CRISPR and SSS methods, we analyzed the *N*-methyl-*D*-aspartate (NMDA) receptor (NMDAR) family comprehensively and found that the *Nr3a* KO mouse is a short sleeper (96.7 min/day less than wild-type). Finally, we developed a freely accessible web-based database that contains the triple-target candidates for 81.2% of the genes in the mouse genome.

## RESULTS

### Triple-Target CRISPR Achieves Almost Perfect KO Efficiency

To obtain a highly efficient method for producing biallelic KO mice, we first constructed a simple computational model to estimate the minimum efficacy of different CRISPR methods (Supplemental Experimental Procedures). According to this computational model, a multiple-target CRISPR strategy, in which multiple gRNAs target the same gene, is more efficient than the high-concentration CRISPR strategy, in which a multiple-fold higher concentration of a single gRNA targets the gene of interest (Figures 1A and 1B; Figures S1A and S1B). This finding is consistent with a previous report on dual-target CRISPR (Zhou et al., 2014). Our model further predicted that triple-target CRISPR would achieve 79%–97% efficiency for the biallelic KO of a single gene (Figure S1C). Importantly, if it achieves more than 90% efficiency for the biallelic KO of a single gene, it can also achieve more than 80% efficiency even for the biallelic KO of dual genes, which is sufficient for reliable analysis of behavioral phenotypes.

To test the model's predictions, we selected *Tyr* as a target gene and C57BL/6N as a basal inbred strain, because if this gene is knocked out biallelically, the black coat color of C57BL/6N becomes white. We designed three gRNAs for three target sequences of the *Tyr* gene (gRNA1, gRNA2, and gRNA3 for targets Tyr-1, Tyr-2, and Tyr-3, respectively; Figures 1C and S1D). We confirmed that the designed gRNAs had high cleavage efficiency (~7-fold to ~40-fold compared to control) at least in cellulo by using a single strand annealing (SSA) assay (Figures 1D and S1E), in which the DNA cleavage of a target sequence by the CRISPR/Cas9 system induced the recombination of incomplete fragments of firefly *Luciferase* (*Luc*), resulting in an entire *Luc* gene and enhanced bioluminescence.

We then estimated two parameters of the model, an effective total gRNA concentration compared to the dissociation constant of gRNA ($S$) and a recovery rate of a mutation ($\alpha$). When injected into fertilized eggs, the single-target strategy using each of the three gRNAs alone at 150 ng/μl exhibited only moderate efficacy (36.0%, 54.2%, and 64.7%, for gRNA1, gRNA2, and gRNA3, respectively; Figures 1F and S1G). Based on these results, $S$ and $\alpha$ were estimated to be 5.72 and 0.136, respectively. This allowed us to predict the minimum efficacy of the triple-target CRISPR method for whole-body biallelic KO mice as 82.6% (Figure S1F). In fact, the triple-target strategy using the mixture of *Cas9* mRNA (100 ng/μl) and three gRNAs (gRNA1, gRNA2, and gRNA3, each at 50 ng/μl) achieved almost perfect efficiency (97.5%; Figures 1E and 1F). We also performed qPCR of the target region including the CRISPR-target sequence and confirmed that five out of six CRISPR-target regions from two *Tyr* KO mice were not detectable. These qPCR results matched with each other among the genomic DNAs extracted from brains, scalps, and tails (Figure S1H), which is consistent with the observed whole-body biallelic KO phenotype (i.e., white coat color) of the *Tyr* gene. We noted that observed KO efficacy (97.5%) is more than the predicted minimum efficiency (82.6%) (Figure S1F). We speculated that the increased KO efficacy would be because of irreversible mutations such as deletion between multiple CRISPR target sites.

To investigate its genomic effect, we performed exome sequencing; results were that 91.6%–95.6% of target bases were covered more than ten times (Table S5). As a result, it demonstrated on-target deletions of genomic stretches with variable lengths (Figure 2) and no off-target mutation. Thus, the

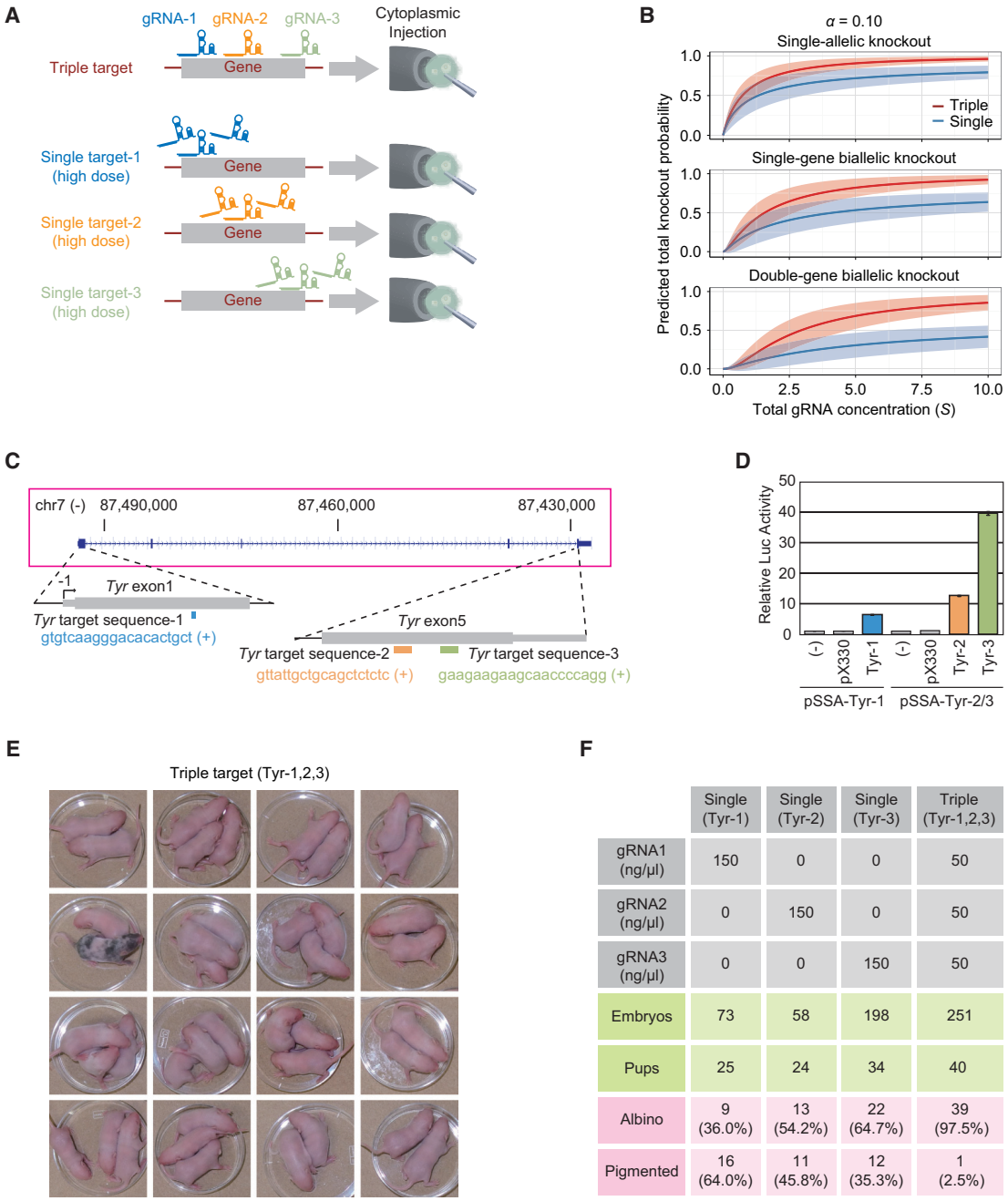


F

| | Single (Tyr-1) | Single (Tyr-2) | Single (Tyr-3) | Triple (Tyr-1,2,3) |
|---|---|---|---|---|
| gRNA1 (ng/μl) | 150 | 0 | 0 | 50 |
| gRNA2 (ng/μl) | 0 | 150 | 0 | 50 |
| gRNA3 (ng/μl) | 0 | 0 | 150 | 50 |
| Embryos | 73 | 58 | 198 | 251 |
| Pups | 25 | 24 | 34 | 40 |
| Albino | 9 (36.0%) | 13 (54.2%) | 22 (64.7%) | 39 (97.5%) |
| Pigmented | 16 (64.0%) | 11 (45.8%) | 12 (35.3%) | 1 (2.5%) |

**Figure 1. A Triple-Target CRISPR Method for Highly Efficient Production of Whole-Body Biallelic KO Mice**

(A) Schematic diagram of triple-target and single-target CRISPR methods. Each method uses the same amount of total gRNA.

(B) Computational simulation predicting how efficiently one or more alleles are cut out when different numbers of gRNAs are used against the same target gene. The triple-target (red line) and single-target (blue line) methods were compared. The line and shaded area around the line indicate the mean and the SD of 1,000 simulations, respectively. The difference in efficiency between triple-target and single-target strategies became more apparent as the number of target alleles increased.

(C) Target sequences of the gRNAs for KO of the *Tyrosinase* (*Tyr*) gene. The short colored bars (blue, orange, and green) indicate the 20-base target sequences. The target sequences were on the sense strand of the genomic DNA (plus sign refers to the gene's sense strand).

(D) SSA assay for the gRNAs of the *Tyr* gene. Relative luciferase activities from the SSA vectors (pSSA-Tyr-1 and pSSA-Tyr-2) were measured. The SSA vector was transfected into 293T cells with empty vector (-), pX330 *Cas9* vector without any gRNA, or pX330 *Cas9* and *Tyr* gRNA (Tyr-1, Tyr-2, or Tyr-3). The relative Luciferase activity for each sample was scaled so that the activity with empty vector (-) was defined as 1. Error bars represent SD (n = 3).

(E) *Tyr* KO mice created by the triple-target CRISPR method. The coat color showed the biallelically knocked out mice.

(F) Comparison of the single- and triple-target CRISPR methods. The table shows the gRNA injection condition and resulting phenotypes (Figure S1G). Embryos, number of injected and transferred embryos; Pups, number of pups born (total); Albino, pups with albino coat color (biallelic knockout); Pigmented, pups with mosaic or wild-type coat color.

Please cite this article in press as: Sunagawa et al., Mammalian Reverse Genetics without Crossing Reveals *Nr3a* as a Short-Sleeper Gene, Cell Reports (2016), http://dx.doi.org/10.1016/j.celrep.2015.12.052



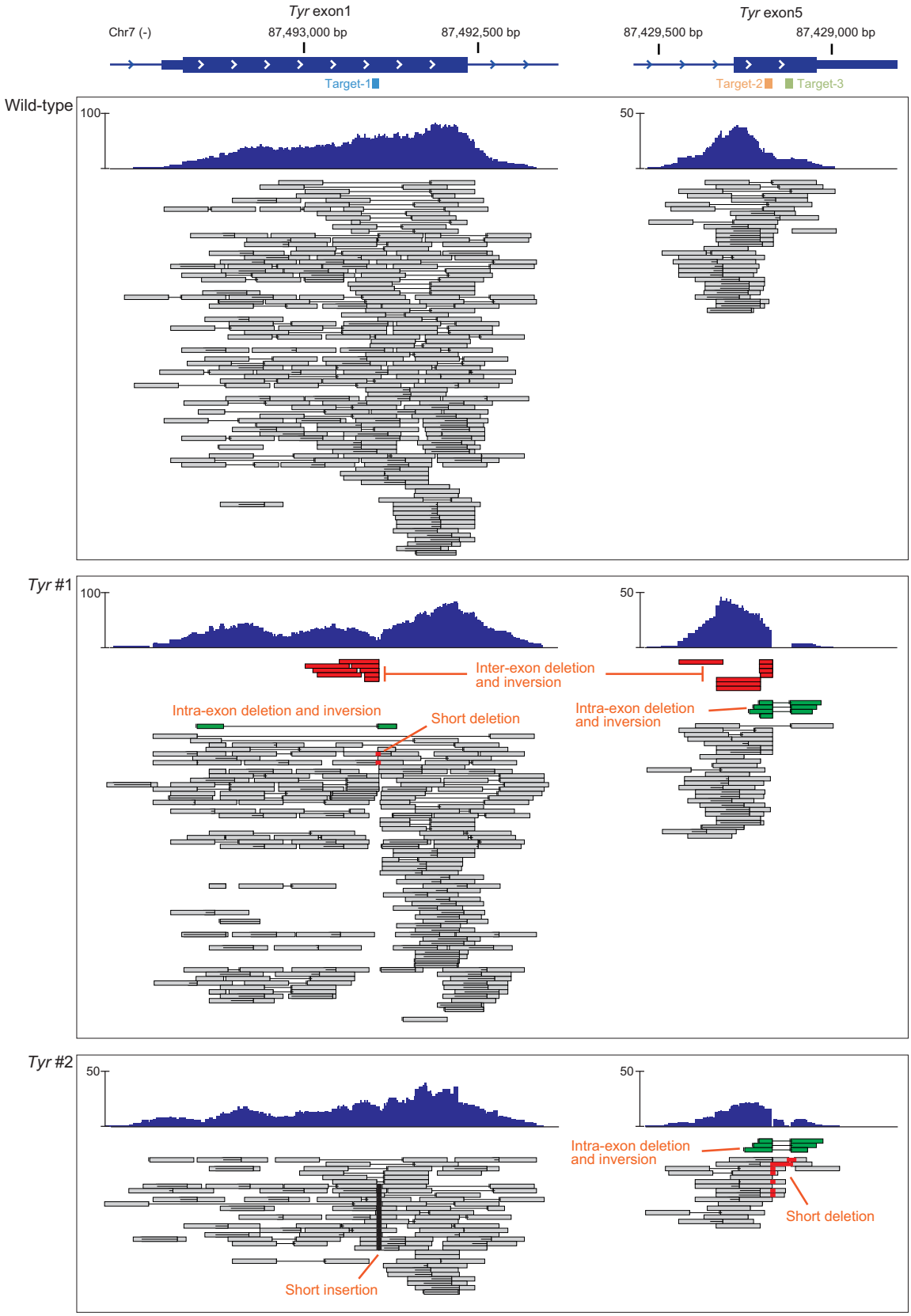


*(legend on next page)*

triple-target CRISPR method could produce biallelic KO mice with >90% efficiency in a single generation. Furthermore, undetectable expression of TYR protein was confirmed by mass spectrometry (MS) comparing with another independently produced triple-target CRISPR KO strain. TYR protein was not detectable in two *Tyr* KO mice, whereas it was detected in one *Nr3a* KO mouse (Figure S1I). Importantly, since a triple-target CRISPR method achieves high efficiency (>90%) for the biallelic KO of a single gene, it has a potential to achieve efficiency higher than 80% even for the biallelic KO of dual genes, which is sufficient for reliable analysis of behavioral phenotypes.

## The SSS Enables Non-invasive, Fully Automated, High-Performance Sleep/Wake Phenotyping

To identify system-level molecular circuits in organisms, both the efficient production of KO mice and simple but accurate phenotyping are necessary. The standard method for phenotyping mammals' sleep/wake states is to record EEG/EMG data. Each short-period segment of EEG/EMG data, called an "epoch," is then annotated into one of three sleep/wake states ("REM [rapid eye movement] sleep," "NREM [non-REM] sleep," and "awake"), determined by the EEG/EMG pattern (Figure S2A). Here, to obtain a non-invasive and fully automated method for simple and accurate sleep/wake phenotype analysis, we developed the SSS (Figure 3A). For this method, we first focused on the non-invasive phenotyping of sleep/wake states by recording the respiration of an animal, since the different states exhibit unique respiration patterns (Figure S2A).

Among the current methods for non-invasively recording the respiration of mice (Glaab et al., 2007; Gordon and Ali, 1984), whole-body plethysmography (WBP) is one of the most popular and promising. The correlation between respiration patterns and EEG/EMG-based sleep/wake states was previously analyzed (Hernandez et al., 2012). However, previous studies mainly examined short recording periods (less than 1 day) during different states of consciousness, so the volume of the WBP chamber could be relatively small. Although a smaller chamber size increases the sensitivity of the respiration recording, too small a chamber decreases the animal's comfort and can affect sleep/wake behavior. Therefore, no system has been developed for recording for a week or more, which is critical for accurate sleep/wake phenotyping. Increasing the size of the chamber requires a compensatory increase in the signal/noise ratio of the WBP system itself.

To optimize the WBP system, we modeled it as an equivalent electrical circuit (Figure 3B; Supplemental Experimental Procedures for the detailed equations)—essentially a band-pass filter for a certain frequency of pressure change. By computer simulation, we optimized the resistance and capacitance in the WBP system to band-pass the 1- to 10-Hz flow (Figure 3C), which is the physiological range for mouse respiration frequency. Based on this analysis, we constructed a high-performance WBP system (Figure 3A), which exhibited a high signal/noise ratio for the 1- to 10-Hz flow and allowed us to record detailed, long-term respiration patterns of mice non-invasively.

For simple and accurate sleep/wake phenotype analyses, fully automated annotation of the recorded data is also critical. We previously developed FASTER (an unsupervised fully automated sleep staging method for mice based on EEG/EMG recordings) (Sunagawa et al., 2013), which avoids the subjective manual annotation of EEG/EMG data. We applied the FASTER method to the recorded respiration data to create a fully automated annotation pipeline (Figure S2B; Supplemental Experimental Procedures). Each epoch is annotated as either "sleep" or "awake" fully automatically. Since REM state represented only ~5% of the total epochs, which agrees with past documentation (Chemelli et al., 1999), we focused on a two-state classification between sleep and awake states as the first-order approximation in this study. Simultaneous recordings of the respiration flow and EEG/EMG enabled us to estimate the performance of the SSS system (Figure 3D), resulting in the high accuracy of 95.3 ± 0.4% (n = 3) for the respiration-based sleep/wake phenotyping (Figures 3E and S2C). Importantly, the non-invasiveness of the recording and fully automated data analysis minimized the variability and subjectivity of the procedures, thereby making the sleep/wake phenotyping highly reproducible, as indicated by the overlapping probability densities of sleep/wake states among three individuals (Figure 3E). We also note that even "quiet awake," which was defined in this study as the awake state accompanied by the lower 33.3% of EMG values, was annotated accurately (95.3 ± 1.3%; n = 3) by the SSS system (Figure S2D). Therefore, the SSS provides a non-invasive, fully automated method for sleep/wake phenotyping.

High-performance in the SSS system enabled us to obtain various sleep/wake phenotypes based not only on daily sleep time (or awake time) but also on the transition probabilities between sleep and awake states (*s* and *w*, respectively, in $P_{ws}$ and $P_{sw}$; Figure 3F) and on the sleep/wake amplitude, which is related to the sleep-time variation within the daily sleep cycle (Figure 3G; Supplemental Experimental Procedures). We note that $P_{ws}$ and $P_{sw}$ were proposed to represent sleep drive and wake drive in a previous study (De Valck and Cluydts, 2003) and that they are informative sleep/wake phenotypes. We also defined the sleep/wake amplitude as the coefficient of variation (CV, the SD divided by the mean) of sleep time for each 10-min bin for 24 hr (Figure 3G).

To evaluate the performance of the SSS system, we recorded 108 individual C57BL/6N male mice (6 weeks old) in the SSS chamber for a week (Figure 3H; Table S1). To avoid the first-day effect, the recorded data from the second day to the seventh day were analyzed by the SSS annotation pipeline. The results revealed a daily sleep time of 735.7 ± 50.8 min (mean ± SD; n = 108), which corresponded to a CV of 6.9%. The $P_{ws}$ and $P_{sw}$ were 0.0379 ± 0.0068 and 0.0363 ± 0.0067, respectively,

**Figure 2. Exome Analysis of Whole-Body Biallelic *Tyr* KO Mice Produced by Triple-Target CRISPR Method**

Genome alignments of exome sequence reads. The genomic regions targeted by the three gRNAs were shown for wild-type, *Tyr* KO #1, and *Tyr* KO #2. The upper part of each panel shows read coverage, and the lower part shows read alignments (rectangles). Horizontal lines between rectangles indicate read pairing. Different types of mutations occurring at the target sites are highlighted as follows: inter-exon deletion and inversion (red rectangles); intra-exon deletion and inversion mutation (green rectangles); short deletion (red dots); and short insertion (black dots).

Please cite this article in press as: Sunagawa et al., Mammalian Reverse Genetics without Crossing Reveals *Nr3a* as a Short-Sleeper Gene, Cell Reports (2016), http://dx.doi.org/10.1016/j.celrep.2015.12.052



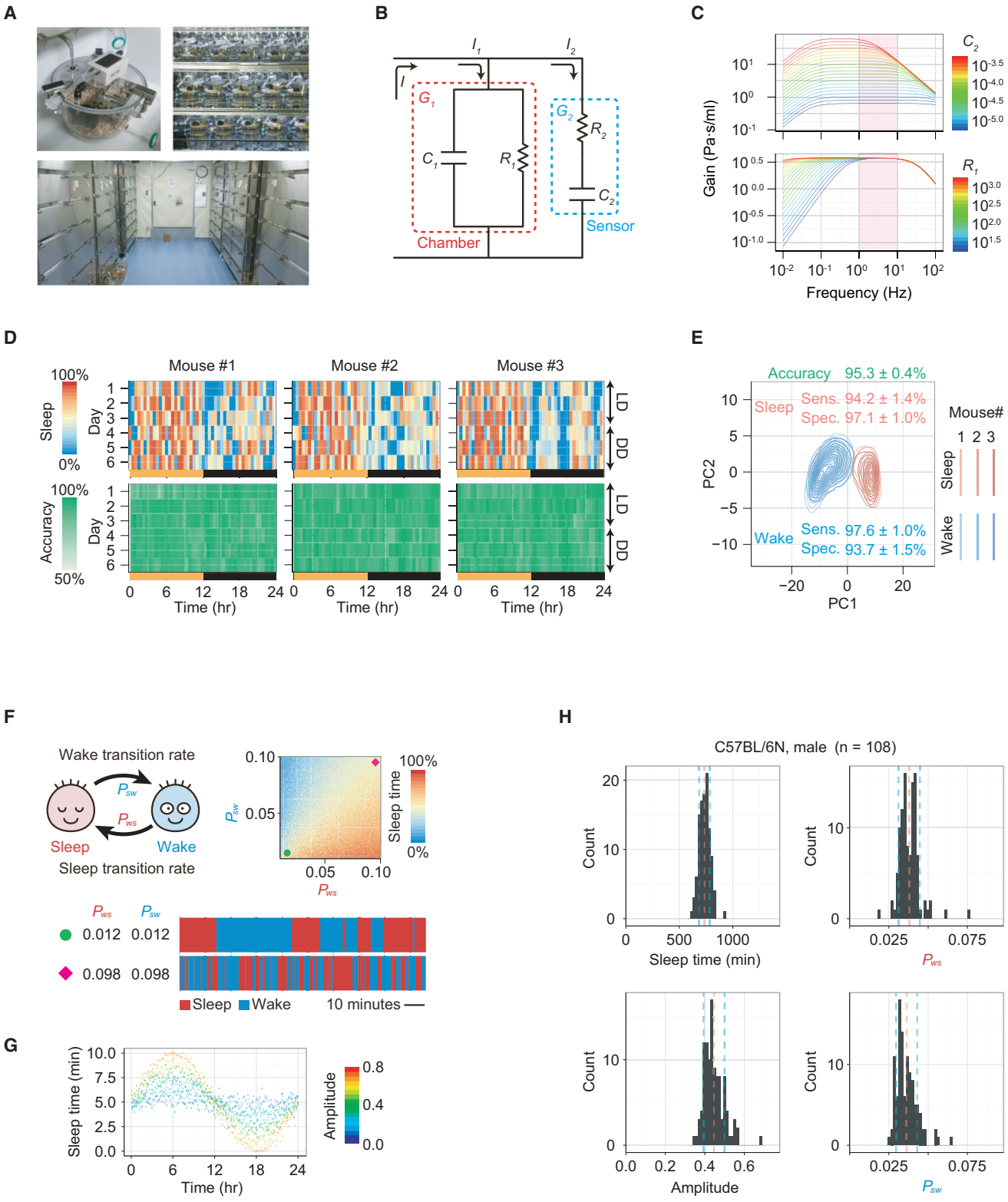


**Figure 3. The SSS Enables Non-invasive, Fully Automated, High-Performance Sleep/Wake Phenotyping**

(A) The SSS system. Upper left: one mouse is housed in an SSS chamber. The chamber is connected to a water outlet, and food is stored in its ceiling, which allows 14 days of continuous recording without additional handling of the chamber. Upper right: up to 36 SSS chambers are set in an SSS rack. The rack is

*(legend continued on next page)*

and the sleep/wake amplitude was 0.4462 ± 0.0530. To evaluate the SSS system for other inbred strains and in females, we recorded C57BL/6J male mice, C57BL/6N female mice, and C57BL/6J female mice (n = 178, 72, and 173, respectively; Figure S2E; Table S1). Their tight distributions of sleep time showed that the SSS provides a simple and high-performance method for sleep/wake phenotyping.

To further validate the SSS, we recorded various known sleep/wake phenotypes in mice. First, we tested mice whose sleep/wake behavior was perturbed pharmacologically. Methamphetamine (MAP), a potent psychostimulant that promotes wakefulness (Edgar and Seidel, 1997), was injected intraperitoneally (i.p.) into mice during the day, at zeitgeber time 2 (ZT2; Figure S3A). The administration of 3 mg/kg MAP significantly decreased sleep time and $P_{ws}$ (Figures S3B and S3C). These results indicated that the decreased sleep time was due to increased stabilization of the awake state rather than by decreased stabilization of the sleep state.

To test the SSS system for the opposite phenotype (sleep-time increase), we injected i.p. a sleep-inducing drug, diazepam (DZP) (Radulovacki et al., 1984), at nighttime, ZT13 (Figure S3D). Indeed, the administration of 5 mg/kg DZP significantly increased the sleep time and $P_{ws}$ (Figures S3E and S3F), which is the exact opposite phenotype observed in MAP injection. To further confirm observed sleep-phenotype changes, we performed the drug administration experiment under simultaneous recording of SSS and EEG/EMG (Figures S3H and S3I). The accuracy, sleep sensitivity, sleep specificity, wake sensitivity, and wake specificity of SSS against EEG/EMG-based sleep staging were as high as those for wild-type animals (Figures 3D and 3E). These results clearly show that SSS is highly sensitive to sleep/wake pattern, even in animals under drug administration.

Furthermore, to test the SSS system's ability to detect the sleep/wake phenotypes of genetically modified animals, we recorded the behavior of circadian mutants that lose their circadian rhythm under constant darkness (DD) (Laposky et al., 2005; Shiromani et al., 2004; Wisor et al., 2002). Three KO strains, *Bmal1* KO (Shimba et al., 2011), *Cry1*/*Cry2* (van der Horst et al., 1999), and *Per1*/*Per2* double-KO mice (Bae et al., 2001) were recorded for a week under LD conditions (light on at ZT0, light off at ZT12; Figure S3J). All strains exhibited less sleep during the light phase (an inactive phase of wild-type mice) and more sleep during the dark phase (an active phase for wild-type mice; Figure S3K). Both $P_{ws}$ during the light phase and $P_{sw}$ during the dark phase are decreased in *Bmal1* KO and *Cry1*/*Cry2* double-KOs (Figures S3L and S3M). Although *Per1*/*Per2* double-KO mice did not exhibit a significant decrease of sleep/wake amplitude, their daily sleep/wake patterns differed from those of wild-type mice (Figure S3K). In all strains, the total sleep time was not significantly different from that of the C57BL/6N mice (Figure S3M; Table S1). Overall, these results also indicate that the SSS can sensitively detect various sleep/wake phenotypes, including the total sleep/wake time, transition probabilities between sleep and awake states, and sleep/wake amplitude.

## Combined Use of a Triple-Target CRISPR and SSS Enables Sleep/Wake Phenotyping, Even in Double-KO Mice

To test the feasibility of combining efficient KO mouse production with automated sleep/wake phenotyping, we analyzed sleep/wake phenotypes in different KO mouse lines produced by the triple-target CRISPR method described earlier. First, we designed three gRNAs against the *Bmal1* gene (Figure S4A). Sleep/wake phenotyping was performed for animals with the KO genotype, which was confirmed by qPCR and/or genomic sequencing (Figures S4D and S4E; Tables S1 and S2). As expected, the generated *Bmal1* KO mice showed a significantly decreased sleep/wake amplitude under LD conditions compared with wild-type mice, and the *Tyr* KO mice did not (Figures 4A–4C; Figure S4H). In contrast, the daily sleep times did not differ between the *Tyr* KO and *Bmal1* KO mice or in comparison with wild-type mice (Figure 4C). Notably, the *Tyr* KO mice had sleep/wake patterns similar to those of the wild-type mice (Figure 4B), indicating that the triple-target CRISPR method itself had little effect on sleep/wake phenotypes. Next, we generated double-KO mice for *Cry1*/*Cry2* and *Per1*/*Per2*, which are well-known mouse clock genes. We designed three gRNAs each for each gene (Figures S4B and S4C), and sleep/wake

equipped with continuous air circulation units, which provides fresh air to each chamber. Lower panel: we used six SSS racks for recording and thus could determine the sleep/wake phenotypes of 216 mice per week.

(B) Equivalent electric circuit model of the SSS system. The SSS chamber (red dashed box) was modeled with a capacitor ($C_1$) and resister ($R_1$) in parallel, and the pressure sensor (blue dashed box) was modeled with the resister ($R_2$) and capacitor ($C_2$) in series (Supplemental Experimental Procedures).

(C) Calculation of the conductance over $R_2$, which corresponds to the amplification factor of the pressure detected with the sensor and optimization of $C_2$ and $R_1$ to maximize the gain of the frequency band of the physiological respiration of mice (1 to 10 Hz, pink shaded area). Based on the simulation results, $C_2$ was fixed to $6.12 \times 10^{-5}$ ml/Pa, and $R_1$ was fixed to 172 Pa • s/ml.

(D) SSS-based sleep/wake staging results compared with conventional EEG/EMG-based sleep/wake staging results. Data from three mice were used. Upper graph shows the sleep time for every 30 min evaluated by SSS. Lower graph shows the accuracy based on conventional EEG/EMG-based staging, for each 30 min during recording.

(E) The performance of SSS. Sleep (red) and awake (blue) states of three individual mice are shown as probability densities on a two-dimesional principal-component map in the SSS annotation pipeline. Values represent the mean ± SD (n = 3) of the sensitivity and specificity of sleep (red) and awake (blue) states when compared with EEG/EMG-based sleep/wake staging. The overall accuracy reached 95.3% ± 0.4% (mean ± SD, green).

(F) Illustration of sleep/wake transitions. Upper left: schematic view of the transition probabilities between sleep and awake states. Upper right: sleep time at different values of $P_{ws}$ and $P_{sw}$. When both $P_{ws}$ and $P_{sw}$ decrease (green circle), both sleep and awake episodes will stabilize. Note that when both $P_{ws}$ and $P_{sw}$ increase (red diamond), the stability of each state is dramatically decreased (bar chart below) without changing the total sleep (or awake) time.

(G) Illustration of sleep/wake amplitude. In the chart, different amplitudes are distinguished by color, and the points represent sleep times at various times of day.

(H) Distribution of sleep/wake parameters of C57BL/6N male mice recorded in the SSS. The pink and sky blue dashed lines show the mean and the mean ± SD of each distribution, respectively.

See also Table S1 and Supplemental Experimental Procedures.

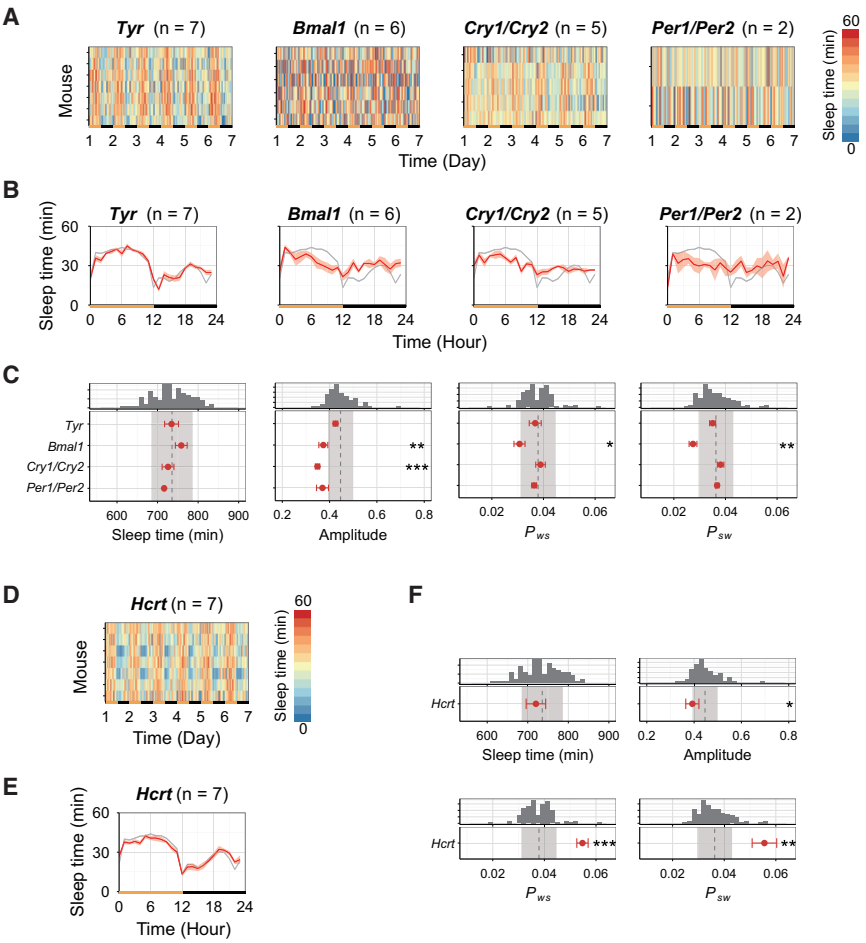


**Figure 4. Combined Use of a Triple-Target CRISPR and SSS Enables Sleep/Wake Phenotyping in Single- and Double-KO Mice**

(A) Sleep time (per hour) phenotype for individual mice in *Tyr* KO mice and circadian-clock mutants produced by triple-target CRISPR.

(B) Sleep time (per hour) over 24 hr averaged over 6 days in *Tyr* KO mice and circadian-clock mutants produced by triple-target CRISPR. Red lines show the mean sleep time at each time of day for each strain. Gray line shows the data for C57BL/6N male mice (n = 108). The shaded area around the line is the SEM for each time point.

(C) Distributions of sleep/wake parameters of *Tyr* KO mice and circadian-clock mutants. Dunnett's test compared to C57BL/6N male mice.

(D) Sleep-time (per hour) phenotype of *Hcrt* KO mice.

(E) Sleep time (per hour) over 24 hr averaged over 6 days in *Hcrt* KO mice. Red line, gray line, and the shaded area are the same as described in (B).

(F) Distributions of sleep/wake parameters of *Hcrt* KO mice. Dunnett's test compared to C57BL/6N male mice. See also Table S1.

phenotyping was performed for animals with the KO genotype (Figures S4F and S4G; Tables S1 and S2). Both strains showed similar phenotypes with conventionally generated KO mice (Figures 4A–4C; Table S1). All three circadian KO strains were also recorded for a week under DD conditions and confirmed to exhibit arrhythmic phenotype (Figures S4I and S4J).

To further validate the functionality of our strategy, we designed three gRNAs against the *Hcrt* gene (Figure S4K) and produced animals by triple-target CRISPR method. Sleep/wake phenotyping was performed for animals with KO genotype (Figure S4L; Tables S1 and S2). Consistent with the conventional *Hcrt* KO mice (Chemelli et al., 1999), the mice showed significant increase in both transition probabilities, $P_{ws}$ and $P_{sw}$, without any significant change in total sleep time (Figures 4D–4F and S4M).

Overall, the combinatorial use of triple-target CRISPR and SSS enables the efficient generation of KO mice and their accurate sleep/wake phenotyping not only in single-KO mice but also in double-KO mice.

## Reverse Genetics without Crossing Reveals *Nr3a* Mutant to Be a Short-Sleeper Mouse

Mammalian reverse genetics without crossing can be applied to the comprehensive analysis of gene functions at the systems and whole-organism level. To demonstrate proof of concept, we comprehensively targeted the members of the NMDAR family. We focused on this family because the NMDAR is implicated in several psychological disorders, including schizophrenia (Belforte et al., 2010; Moghaddam and Javitt, 2012; Mohn et al., 1999), Alzheimer's disease (Snyder et al., 2005), and depression (Autry et al., 2011; Li et al., 2010), all of which have associated sleep disorders.

There are seven genes in the NMDAR family: *Nr1*, *Nr2a*, *Nr2b*, *Nr2c*, *Nr2d*, *Nr3a*, and *Nr3b*. For triple-target CRISPR, we designed three gRNAs for each of these genes (Figures S5A–S5G) and used them to generate KO mice for each one. Sleep/wake phenotyping was performed for animals with the KO genotype, which was confirmed by qPCR and/or genomic sequencing (Figures S5H–S5L; Tables S1 and S2). First, we confirmed that the lethal phenotype seen in *Nr1* and *Nr2b* bialelic KO mice that was generated by conventional methods (Forrest et al., 1994; Li et al., 1994) also occurred in *Nr1* and *Nr2b* KO mice generated by the triple-target CRISPR method, because we noted that there were no survivors of *Nr1* and *Nr2b* KO genotypes (Table S2). KO mice for the other five NMDAR genes, *Nr2a*, *Nr2c*, *Nr2d*, *Nr3a*, and *Nr3b*, survived for at least 6 to 7 weeks (Table S2), at which time they were placed in SSS chambers, and their sleep/wake behavior was recorded for at least 1 week under LD conditions. For the phenotype analysis, we used the 6-day data from the second recording day to avoid the first-day effect (Figure 5A). The sleep/wake phenotype analysis was performed fully automatically, and the statistical evaluation used sleep time, $P_{ws}$, $P_{sw}$, and sleep/wake amplitude as parameters (Figures 5B, 5C, and S5M; Table S1).

Among the five KO mice, the *Nr3a* KO mice showed a significant "short-sleeper" phenotype, with a daily sleep time of

639.0 ± 17.5 min (n = 8), which is 96.7 min shorter than that of wild-type mice ($p < 0.0001$). *Nr3a* KO mice displayed a lower $P_{ws}$ than wild-type mice, whereas their $P_{sw}$ was normal (Figure 5C), indicating that their short-sleeper phenotype was due to an increase in awake-state stabilization (i.e., longer episode durations of the awake state) but not a decrease in sleep-state stabilization. To preclude the possibility of an off-target effect of CRISPR/Cas9 gene editing, we generated another group of *Nr3a* KO mice (n = 12) by an independent CRISPR probe set (set 2; Figures S6A and S6B; Table S2) and confirmed the observed short-sleeper phenotype compared with wild-type mice ($p < 0.0001$) (Figures 5D–5F and S6C). Furthermore, to ensure that the short-sleeper phenotype is not due to the modality of sleep evaluation, we produced another series of *Nr3a* (set 1) KO mice (Figure S6D) and used EEG and EMG recordings to evaluate their sleep. Consistent with the SSS results, EEG recordings showed a significant short-sleeper phenotype in KO mice ($p < 0.05$; Figure S6E). For genomic validation, four of the generated *Nr3a* KO mice (Figures S5K and S6B) mentioned earlier were analyzed with exome sequencing (Table S5). In both set 1 and set 2 animals, the analysis revealed deletions of genome stretches with variable lengths at the target site (Figure 6; Figure S7A), with its extent for at least one target site of up to 100% (see Figure S7B for a magnifiable view). Importantly, no off-target mutation was identified in this exome sequencing. These results strongly suggested that the observed short-sleeper phenotype of *Nr3a* KO mice cannot be attributed to the possible off-target effect of CRISPR but rather to the common genomic defects in the *Nr3a* gene. Finally, to confirm the absence of NR3A protein in the KO animals, we have performed MS analysis in these animals (Figure S6F). Two *Tyr* KO animals (Figure S4D) were used as controls for NR3A protein detection, which showed a clear peak at the position of internal standard of NR3A protein. By contrast, none of the *Nr3a* KO mice (Figures S5K and S6B) had a detectable peak at the position of internal NR3A protein. These results suggest that *Nr3a* is knocked out not only at the genomic level but also at the protein expression level. Overall, these results demonstrate that the use of mammalian reverse genetics without crossing, and specifically combining this efficient KO mouse production with accurate, automated phenotyping, enables the comprehensive identification of shared and diverse functions of gene family members in organisms.

### Developing a Database for the Triple-Target CRISPR Method

As described earlier, triple-target CRISPR enabled us to efficiently produce biallelic KO mice. However, as we produced several KO mice using this method, we noticed that manually designing triple targets for the same gene is still time consuming, even using existing tools to extract candidate target sequences for a given genomic sequence (http://cas9.cbi.pku.edu.cn/index.jsp) (Ma et al., 2013) and to evaluate the off-target risk for each candidate (http://tools.genome-engineering.org) (Ran et al., 2013). This manual design procedure takes up to a few hours for a single gene and, therefore, limits the ability to perform large-scale screenings. Therefore, we sought to develop an automated method that performs all of the gRNA selection steps. We scanned the whole mouse genome once, and all of the suitable targets are now in an online database (Figure 7A; Supplemental Experimental Procedures). This gRNA database provides at least three target sequences (one set for triple-target CRISPR) for 81.2% of mouse genes. In addition, 71.9% of all mouse genes have more than six target sequences (multiple sets for triple-target CRISPR), which are also included (Figures 7B and 7C).

To validate the usefulness of the triple-target CRISPR database, we selected two independent sets of triple targets for the *Tyr* gene (Tyr-4, Tyr-5, and Tyr-6 for set 2, and Tyr-7, Tyr-8, and Tyr-9 for set 3; Figure 7D), which were distinct from Tyr-1, Tyr-2, and Tyr-3 (set 1) used in the previous experiments (Figure 1C). When injected into fertilized eggs, the triple-target method using both sets of gRNAs showed almost perfect efficacy (96.6% and 100%, respectively; Figures 7E and 7F), supporting the usefulness of the triple-target CRISPR database. Therefore, we made this database public (http://crispr.riken.jp/).

## DISCUSSION

### Triple-Target CRISPR Enables the Efficient Production of Biallelic KO Mice in a Single Generation

In this study, we sought to achieve the highly efficient (>90%) production of whole-body biallelic KO mice in a single generation. We used a simple computational model to estimate the minimum efficacy of different CRISPR methods and discovered that multiple-target CRISPR methods would generate mutant mice with much higher efficiency than single-target CRISPR. We designed three different gRNAs against the *Tyr* gene and confirmed that the triple-target CRISPR method—using a mixture of three gRNAs (Tyr-1, Tyr-2, and Tyr-3)—achieved almost perfect efficacy (97.5%), whereas the single-target method with any of the gRNAs at a 3-fold higher concentration had only moderate efficiency. Genomic verification revealed no off-target mutation, at least in exons (Figure 2; Table S5). The total number of gigabase pairs (or Gbp) read in the exome sequencing including *Tyr* (set 1), *Nr3a* (set 1), and *Nr3a* (set 2) KOs was 65.6 Gbp. This is more than 24 times greater than the whole genome base pairs of mouse (2.7 Gbp). This, therefore, gives us enough coverage to be confident that off-target effect of the triple-target CRISPR strategy is not a problem in practice. Importantly, the DNA-cleavage efficiency of Tyr-3 was more than 3-fold higher than that of Tyr-2 (Figure 1D), whereas the whole-body biallelic KO efficiency for Tyr-3 (64.7%) was similar to that for Tyr-2 (54.2%) (Figure 1F), indicating that a limiting factor in vivo is not DNA cleavage by the CRISPR/Cas9 system but other factors such as DNA repair, consistent with the prediction by the computational model. The reproducibility and robustness of the triple-target method were further confirmed by additional experiments with two independent sets of three gRNAs against the *Tyr* gene (Figures 7E and 7F). We also confirmed the KO efficiency by genotyping all mice used for SSS analysis in this study. We genotyped 102 mice produced by the triple-target CRISPR method, including 11 single-KO and 2 double-KO strains (Table S2). At least 92.2% (n = 94) of the animals were confirmed as KO mice by qPCR or sequencing. This efficacy is confirmed to be higher than the minimum efficacy predicted by our model. In addition, the triple-target CRISPR method is scalable and can be applied to the identification of common and

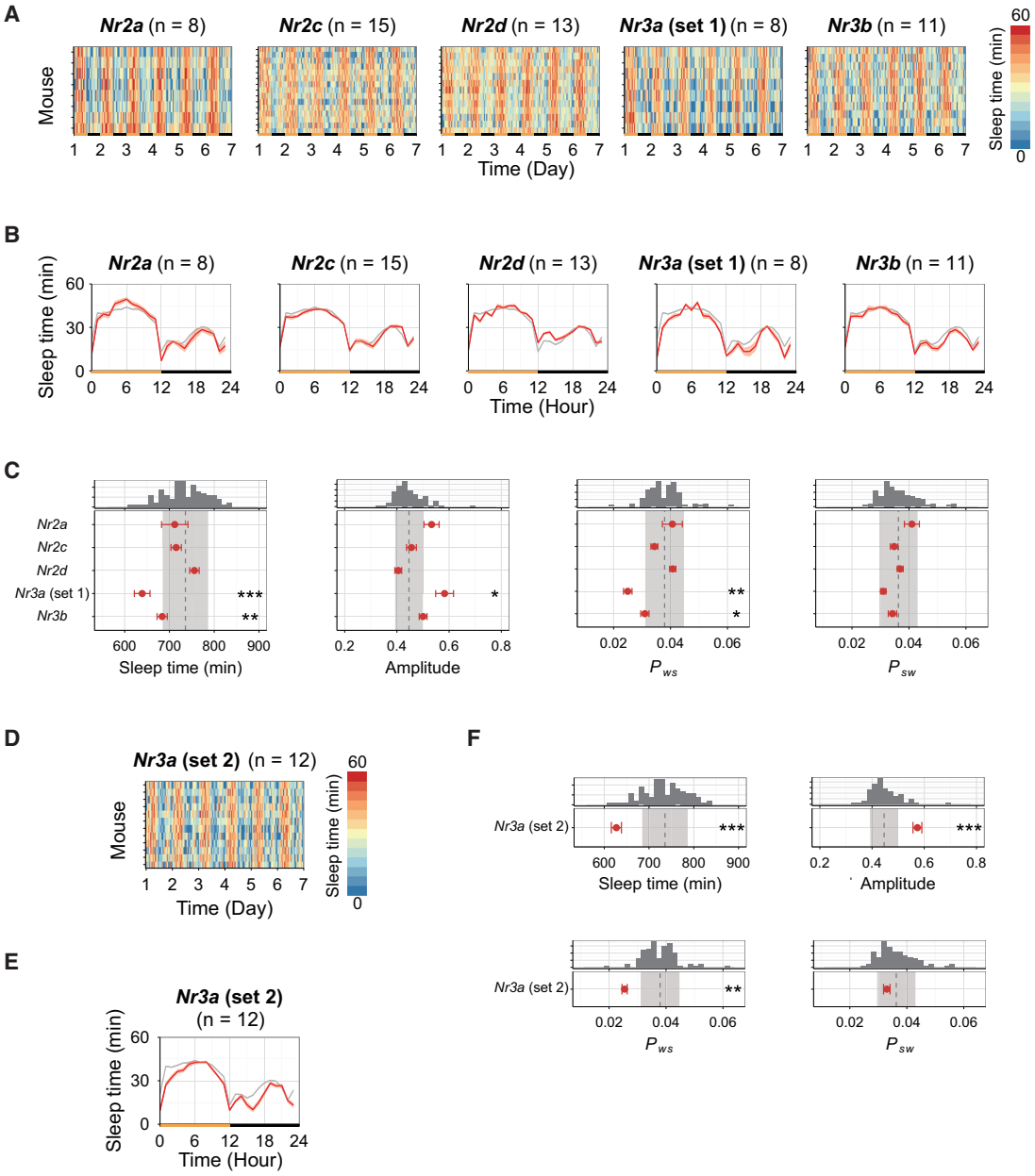


**Figure 5. Reverse Genetics without Crossing Reveals *Nr3a* Mutant to Be a Short-Sleeper**

(A) Sleep-time (per hour) phenotype for all individual KO mice of five NMDA receptor family members generated by triple-target CRISPR.

(B) Sleep time (per hour) over 24 hr, averaged over six days in KO mice of five NMDA receptor family members. Red lines show the mean sleep time at each time of day for each strain. Gray line shows the data for C57BL/6N male mice (n = 108). The shaded area around the line is the SEM for each time point.

(C) Distributions of sleep/wake parameters of comprehensive KO mice of NMDA receptor family members. Dunnett's test or Dunnett's modified Tukey-Kramer pairwise multiple comparison test compared to C57BL/6N male mice.

(D) Sleep-time (per hour) phenotype of *Nr3a* KO mice (set 2) generated by triple-target CRISPR.

(E) Sleep time (per hour) over 24 hr, averaged over 6 days in *Nr3a* KO mice (set 2). Red line, gray line, and the shaded area are the same as described in (B).

(F) Distributions of sleep/wake parameters of *Nr3a* KO mice (set 2). Dunnett's test or Dunnett's modified Tukey-Kramer pairwise multiple comparison test compared to C57BL/6N male mice.

See also Table S1.

diverse functions of a gene family of interest (Figure 5). Furthermore, the triple-target CRISPR method is applicable to the phenotype analysis of double-KO mice (Figures 4A–4C). We also created a publicly available CRISPR database that provides triple-target candidate gRNAs for more than 81.2% of the genes in the mouse genome (Figure 7A).

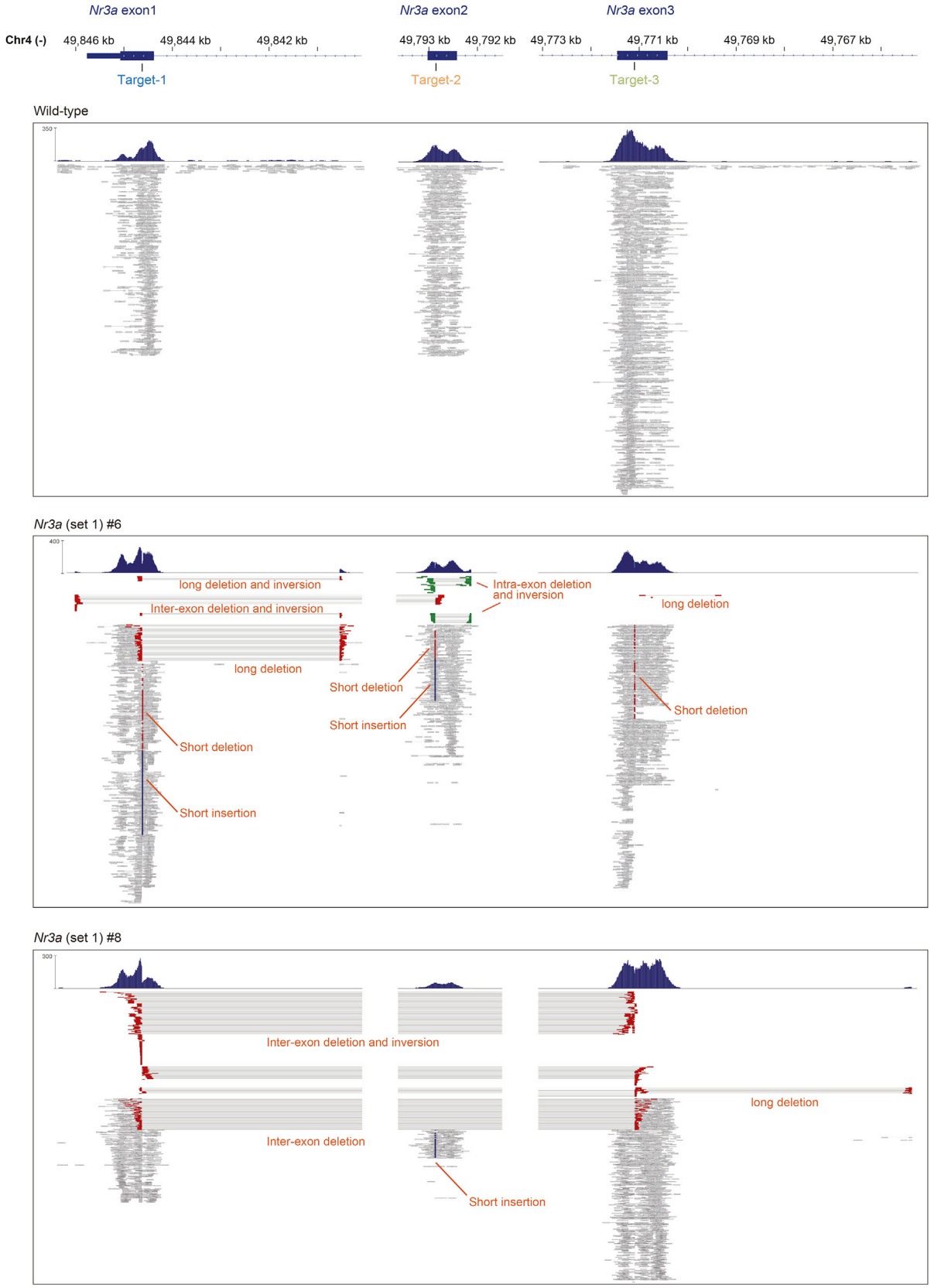


*(legend on next page)*

Please cite this article in press as: Sunagawa et al., Mammalian Reverse Genetics without Crossing Reveals *Nr3a* as a Short-Sleeper Gene, Cell Reports (2016), http://dx.doi.org/10.1016/j.celrep.2015.12.052

## The SSS Provides a Simple and Accurate Phenotyping Method for a Complex Behavior

Along with the efficient production of biallelic KO mice, accurate phenotype analysis is also important to make full use of mammalian reverse genetics without crossing. In this study, we focused on the phenotype analysis of sleep/wake states, because sleep disorders are often associated with psychiatric diseases. The development of a non-invasive and fully automated method for sleep/wake phenotyping (the SSS) allowed us to sensitively detect the sleep-time effects of drugs targeting the CNS, including a psychostimulant, MAP (dopamine transporter antagonist), and a known sleep-inducing drug, DZP ($GABA_A$ receptor agonist) (Figures S3A–S3F). In addition, the SSS enabled us to accurately and quantitatively analyze other sleep/wake phenotypes, such as sleep/wake amplitude, which was shown by the decreased amplitude of clock mutants (Figure 4C), as well as the transition probabilities from sleep to awake states, and from awake to sleep states (Figures 3F–3H), which was clearly shown by the significant increase of $P_{ws}$ and $P_{sw}$ in *Hcrt* KO mice (Figure 4F). This ability is useful for dissecting the effects of CNS drugs on daily sleep time. For example, we found that the decreased sleep time caused by MAP was due to an increase in awake-state stabilization (low $P_{ws}$) rather than to a decrease in sleep-state stabilization (Figure S3B). In contrast, the increased sleep time caused by DZP for 5 hr after the injection was due to a decrease in awake-state stabilization (high $P_{ws}$) (Figure S3E), suggesting that the sleep/wake phenotype induced by DZP is functionally the opposite of that induced by MAP. Interestingly, after DZP increased the sleep time (0 to 5 hr after injection), it conversely decreased the sleep time (5 to 10 hr after injection) (Figure S3G). This compensatory decrease in sleep time by DZP was associated with a slight decrease in sleep-state stabilization (high $P_{sw}$) (Figure S3G; $p = 0.0869$). These results suggest that the SSS can sensitively detect and carefully dissect the common and diverse sleep/wake effects of drugs targeting the CNS.

The sleep time of two circadian KO animals, *Bmal1* KO and *Cry1/Cry2* double-KO mice, recorded in the SSS is not exactly the same as in past reports (Laposky et al., 2005; Wisor et al., 2002). This might be partly because of the functional advantages of the SSS system. First, because of its convenience, the number of recorded mutant mice is larger in this study, where 34 *Bmal1* KO and 27 *Cry1/Cry2* KO mice and more than 100 wild-type mice are recorded. In contrast, nine *Bmal1* KO mice against eight wild-type mice are recorded in the Laposky et al. (2005) paper, and six *Cry1/2* double-KO mice against eight wild-type mice are recorded in the Wisor et al. (2002) paper. Second, in both studies, the sleep phenotypes were evaluated by electrodes implanted in the skull, which is inevitably invasive. In fact, three out of nine KO mice were removed from the study after EEG/EMG recording in the Laposky et al. paper because EEG/EMG signals were deteriorating, which implies some invasiveness inherited in the conventional EEG/EMG recording methods.

Several other approaches have been used in the past to develop automated non-invasive sleep staging systems. The video-based sleep stager is non-invasive and can discriminate between REM and NREM (McShane et al., 2012). However, the expected drawback is difficulty in parallelization due to the huge amount of data to be handled. Furthermore, this method requires a user to set a parameter, which makes it distinct from the SSS, which requires no manual optimization. Piezoelectric-based movement detection technology allowed for estimation of the sleep/wake status from the animal motion (Flores et al., 2007). The simplicity of this system is attractive, although when performing a high-throughput phenotyping in this system, we expect its inevitable interference, i.e., the difficulty in assigning the movement information to the recoding animal against the inevitable noise coming from the neighboring chambers. In contrast, the SSS only uses single-channel respiration flow information per animal, which is a very compact-sized dataset and the respiration is detected only by the pressure inside the chamber, which is much less prone to be affected from the neighboring chambers. These characteristics make the SSS a much useful technology.

## Regulation of Sleep/Wake States by NMDAR Family Members

To test the use of our combined method to comprehensively identify the common and diverse functions of gene family members, we separately knocked out all of the NMDAR family members. We found that *Nr3a* KO mice are short-sleeper mutants. *Nr3a* expression peaks during early postnatal life and decreases to lower levels in adulthood (Henson et al., 2010). Unlike the traditional NMDARs, Nr3a-containing NMDARs have less $Ca^{2+}$ permeability and are almost completely insensitive to $Mg^{2+}$ block at hyperpolarized potentials (Sasaki et al., 2002; Tong et al., 2008). Recently, adult *Nr3a* KO mice were reported to have increased pain sensation and enhanced abilities in learning and memory tasks (Mohamad et al., 2013). These KO mice had greater long-term potentiation (LTP) in adult hippocampal slices compared with wild-type slices. Based on these previous findings, we can assume two possible hypotheses to explain the short-sleeper phenotype in *Nr3a* KO animals. One is the developmental circuit influence of Nr3a-containing neurons. Since *Nr3a* defect impairs fundamental NMDAR responses that are deeply related to formation of synaptic networks, the absence of *Nr3a* may alter the original sleep regulation network of the brain. The other is the direct neural activity modulation by NR3A-containing neurons. Even *Nr3a* impairment during development may be complemented by another mechanism; the influence of *Nr3a* modulation against neural activity remains until adulthood. The enhanced LTP can be explained by decreased blunting of the NMDAR response by *Nr3a*. Because the NMDAR

**Figure 6. Exome Analysis of Whole-Body Biallelic *Nr3a*, Set 1, KO Mice Produced by Triple-Target CRISPR Method**

The genomic regions targeted by the three gRNAs were shown for two mice in *Nr3a* (set 1) KO group (Figure S5K). The upper part of each panel shows read coverage, and the lower part shows read alignments (rectangles). Horizontal lines between rectangles indicate read pairing. Different types of mutations occurring at the target sites are highlighted as follows: inter-exon deletion (red rectangles); intra-exon deletion mutation (green rectangles); short deletion (red dots); and short insertion (blue dots).

Please cite this article in press as: Sunagawa et al., Mammalian Reverse Genetics without Crossing Reveals *Nr3a* as a Short-Sleeper Gene, Cell Reports (2016), http://dx.doi.org/10.1016/j.celrep.2015.12.052



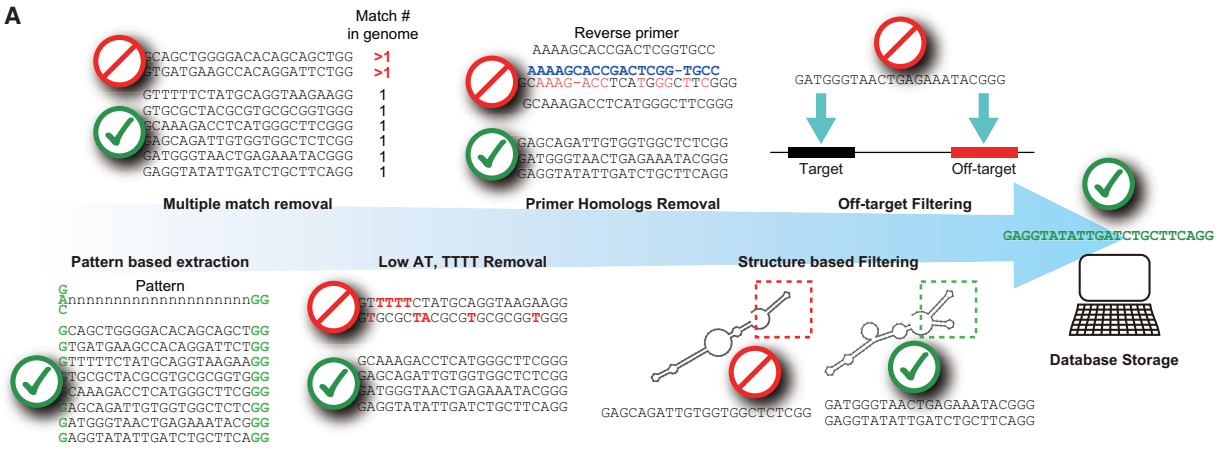


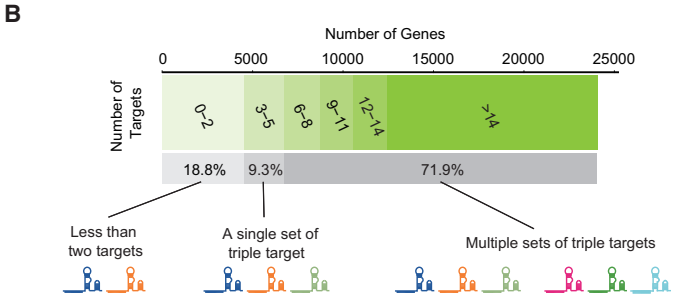


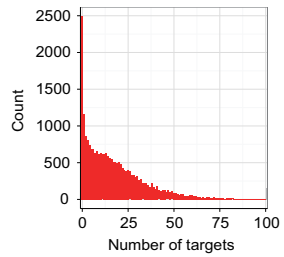


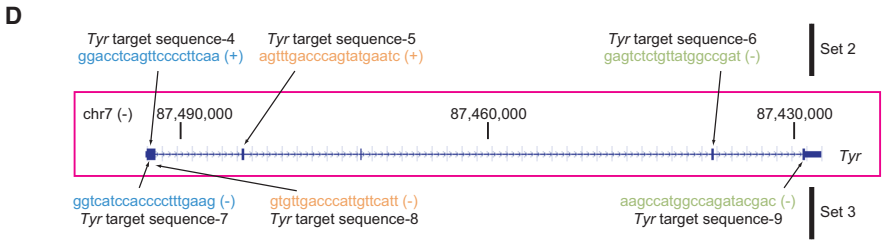


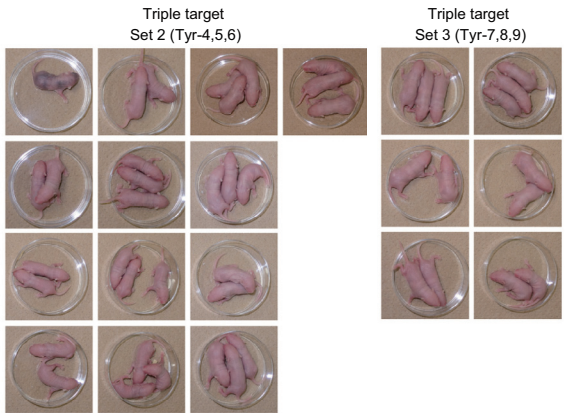


F

| | Triple Set 2 (Tyr-4,5,6) | Triple Set 3 (Tyr-7,8,9) |
|---|---|---|
| gRNA1 (ng/μl) | 50 | 50 |
| gRNA2 (ng/μl) | 50 | 50 |
| gRNA3 (ng/μl) | 50 | 50 |
| Embryos | 145 | 105 |
| Pups | 32 | 14 |
| Albino | 31 (96.9%) | 14 (100%) |
| Pigmented | 1 (3.1%) | 0 (0%) |

*(legend on next page)*

family can be strongly blocked by MK-801, which results in hyperlocomotion when administered to mice (Koek et al., 1988), it is possible that, without *Nr3a*, the NMDAR response is weakened, and this may result in shorter sleep. To test these hypotheses, conditional perturbation of Nr3a-containing neurons is necessary in future investigations.

Although the detailed molecular mechanism, in which *Nr3a* contributes to the sleep/wake cycle, remains to be elucidated, the discovery of *Nr3a* KO mice as a strong short sleeper provides an interesting entry point for mammalian sleep research. We also note that, in the fruit fly, forward genetic screenings have shown that other ion channels play important roles in sleep homeostasis. Mutation in the *Shaker* gene, which encodes a voltage-dependent potassium channel, and in the *Redeye* gene, which encodes a nicotinic acetylcholine receptor $\alpha$ subunit, both result in a short-sleeping phenotype (Cirelli et al., 2005; Shi et al., 2014). Therefore, it will be interesting to investigate the relationship of the mammalian homologs of these channels to NR3A-containing NMDARs in mammalian sleep.

## Toward Organism-Level Systems Biology

In this study, we sought to develop mammalian reverse genetics without crossing by eliciting the efficient (>90%) production and accurate (>90%) phenotype analysis of mutant animals in a single generation. Mammalian reverse genetics without crossing (called "next-generation" mammalian reverse genetics) now allows us to test—in whole organisms—hypotheses that are derived from the past knowledge. For example, a computational model of slow-wave sleep that provides explanations for the observed complex dynamics of sleep/wake states, along with predictions for the important molecular pathways regulating these states, could be extremely powerful. Previously, it was difficult to test such predictions, at least without years of labor. However, the present study demonstrated that the importance of a predicted molecular pathway can be efficiently tested using next-generation reverse genetics. Therefore, one of the next challenges will be to construct a simple computational model and experimentally validate its predictions using triple-target CRISPR and/or the SSS. New research fields, including the system-level identification and analysis of molecular circuits in whole organisms, lie ahead.

## EXPERIMENTAL PROCEDURES

### Animals

C57BL/6NJcl mice were purchased from CLEA Japan, and C57BL/6J mice were purchased from Oriental Yeast. All mice were given food and water ad libitum. They were kept in an environment at an ambient temperature of 21°C, with a relative humidity of 50%. The light was controlled under a 12-hr/12-hr light/dark cycle. All experimental procedures and housing conditions involving animals and their care were in accordance with the RIKEN Regulations for Animal Experiments and the Animal Care and the Use Committee of the Graduate School of Medicine, The University of Tokyo.

### One-Cell Embryo Microinjection

C57BL/6N females (4–6 weeks old) were superovulated and mated with C57BL/6N males. Fertilized eggs were collected from the ampulla of the oviduct of plugged C57BL/6N females by micro-dissection and kept in KSOM medium (Merck Millipore) in a 5% $CO_2$ incubator at 37°C. *Cas9* mRNA (100 ng/μl) and gRNAs (150 ng/μl in total) were co-injected into the cytoplasm of fertilized eggs in M2 medium (Merck Millipore) at room temperature. Details of the cytoplasmic injection were described previously (Sumiyama et al., 2010). After microinjection, the injected embryos were cultured for 1 hr in KSOM medium (Merck Millipore) in a 5% $CO_2$ incubator at 37°C, and 15–30 embryos were then transferred to the oviducts of pseudopregnant ICR female mice.

### Non-invasive Sleep/Wake Phenotype Analysis by SSS Recordings

Mice were placed in the SSS chamber (Figure 3A, upper left panel; Minamide Rika Shokai), which had an air flow of at least 0.4 l/min. The chamber was connected to the SSS sensor (PMD-8203-2G, Biotex, light brown box on top of the chamber in Figure 3A), which detected the pressure difference between the outside and inside of the chamber. The analog signal output from the sensor was digitized at 250 Hz by an AD converter (ADS-0128aK-64MB, Microscience) and stored on a computer by data logging software (Lab-DAQ Pro, Matsuyama Advance). The analysis of the digitized data was fully automated as follows: first, the respiration time domain data were converted to frequency domain data by fast Fourier transformation. The power spectrum was then subjected to principal-component analysis. The first three principal components were used for clustering by probability density clustering (Azzalini and Torelli, 2007). Finally, the clusters were annotated according to the power spectrum of each cluster. The details in each step of SSS annotation pipeline are described in the Supplemental Experimental Procedures. One set of data recording in the SSS chamber was for 2 weeks. During the experiment, neither the chamber nor the rack was opened unless the injection was performed i.p. The light condition of the SSS rack was set to a 12-hr/12-hr light/dark cycle, and food and water were given ad libitum. Data analysis was conducted 6 days from the second recording date.

## SUPPLEMENTAL INFORMATION

Supplemental Information includes Supplemental Experimental Procedures, seven figures, five tables, and a data file showing the source code of the SSS analysis and can be found with this article online at http://dx.doi.org/10.1016/j.celrep.2015.12.052.

## AUTHOR CONTRIBUTIONS

H.R.U. and G.A.S. designed the study. G.A.S. developed the SSS system and performed the sleep data analysis. G.A.S. and S.S. performed the SSS recording. G.A.S., D.T., and K.L.O. performed EEG/EMG recordings. K.S. developed the triple-target CRISPR method. M.U.-T. designed the CRISPR probes. M.U.-T. and S.S. produced CRISPR probes. K.S. and R.O. produced the mice. D.P. implemented the whole-genome detection method and the

**Figure 7. A Publicly Available Database for the Triple-Target CRISPR Method**

(A) The pipeline for automatically selecting targets for the triple-target CRISPR method.

(B) Distribution of the number of the targets per gene.

(C) Histogram of the number of targets per gene.

(D) Alternative target sequences for the *Tyr* gene.

(E) Experimental validation of the automatically selected targets for the *Tyr* gene. Two sets of additional triple gRNAs (Tyr-4, Tyr-5, and Tyr-6 for set 2 and Tyr-7, Tyr-8, and Tyr-9 for set 3) were tested. Photographs show the coat color of the generated mice.

(F) Table shows the injection conditions of the gRNAs and resulting phenotype. Embryos, number of injected and transferred embryos; Pups, number of born pups (total); Albino, pups with albino coat color (biallelic knockout); Pigmented, pups with mosaic or wild-type coat color.

database for the triple-target CRISPR method. H.U. developed the SSA assay. M.U.-T. and H.F. performed the genotyping of animals. O.N. and S.K. performed the exome sequencing analysis. R.N. and Y.S. performed the protein quantification. H.R.U. and G.A.S. wrote the manuscript. All authors discussed the results and commented on the manuscript text.

## ACKNOWLEDGMENTS

We thank T. Mikami for the enthusiastic support for developing the SSS. We also thank all the lab members at RIKEN CDB, QBiC, and The University of Tokyo, in particular, S. Fujino, J. Hara, J. Yoshida-Garcon, M. Shiokawa, A. Kishimoto, A. Nishiyama, A. Sato, Y. Wada, and M. Nomura for their kind help in preparing the materials and supporting experiments; the LARGE, RIKEN CDB for housing the mice; Kaori Tatsumi in the Phyloinformatics Unit (GRAS), RIKEN Center for Life Science Technologies, for exome library preparation and sequencing; T. Ueno for running the initial experiment for triple-target CRISPR; F. Tatsuki and G. Kanda for helpful discussion; and K. Yoshida for improving the SSS algorithm. This work was supported by the Innovative Cell Biology by Innovative Technology Program from the Ministry of Education, Culture, Sports, Science and Technology (MEXT) of Japan (H.R.U.); a Grant-in-Aid for Scientific Research (S) (grant no. 25221004; H.R.U.) and a Grant-in-Aid for Scientific Research on Innovative Areas (grant no. 23115006) from MEXT/Japan Society for the Promotion of Science (JSPS; H.R.U.); a Grant-in-Aid for Young Scientists (B) (grant no. 26870858; G.A.S.); a Grant-in-Aid for Scientific Research on Innovative Areas (grant no. 26113720; K.S.); the strategic programs for R&D (President's discretionary fund) of RIKEN (H.R.U.); an intramural Grant-in-Aid from the RIKEN Center for Developmental Biology and RIKEN Quantitative Biology Center (H.R.U.); a grant from AMED Core Research for Evolutionary Medical Science and Technology (AMED-CREST), Japan AMED (H.R.U.), and Core Research for Evolutionary Science and Technology (CREST), Japan Science and Technology Agency (JST; H.R.U.); the Program for the Brain Mapping by Integrated Neurotechnologies for Disease Studies (Brain/MINDS) from the MEXT (H.R.U.); the Basic Science and Platform Technology Program for Innovative Biological Medicine from the Japan Agency for Medical Research and Development (H.R.U.); and by the RIKEN Foreign Postdoctoral Researcher Program (D.P.).

Received: September 27, 2015
Revised: October 29, 2015
Accepted: December 8, 2015
Published: January 7, 2016

## REFERENCES

Autry, A.E., Adachi, M., Nosyreva, E., Na, E.S., Los, M.F., Cheng, P.F., Kavalali, E.T., and Monteggia, L.M. (2011). NMDA receptor blockade at rest triggers rapid behavioural antidepressant responses. Nature *475*, 91–95.

Azzalini, A., and Torelli, N. (2007). Clustering via nonparametric density estimation. Stat. Comput. *17*, 71–80.

Bae, K., Jin, X., Maywood, E.S., Hastings, M.H., Reppert, S.M., and Weaver, D.R. (2001). Differential functions of mPer1, mPer2, and mPer3 in the SCN circadian clock. Neuron *30*, 525–536.

Belforte, J.E., Zsiros, V., Sklar, E.R., Jiang, Z., Yu, G., Li, Y., Quinlan, E.M., and Nakazawa, K. (2010). Postnatal NMDA receptor ablation in corticolimbic interneurons confers schizophrenia-like phenotypes. Nat. Neurosci. *13*, 76–83.

Carbery, I.D., Ji, D., Harrington, A., Brown, V., Weinstein, E.J., Liaw, L., and Cui, X. (2010). Targeted genome modification in mice using zinc-finger nucleases. Genetics *186*, 451–459.

Chemelli, R.M., Willie, J.T., Sinton, C.M., Elmquist, J.K., Scammell, T., Lee, C., Richardson, J.A., Williams, S.C., Xiong, Y., Kisanuki, Y., et al. (1999). Narcolepsy in orexin knockout mice: molecular genetics of sleep regulation. Cell *98*, 437–451.

Cirelli, C., Bushey, D., Hill, S., Huber, R., Kreber, R., Ganetzky, B., and Tononi, G. (2005). Reduced sleep in Drosophila Shaker mutants. Nature *434*, 1087–1092.

De Valck, E., and Cluydts, R. (2003). Sleepiness as a state-trait phenomenon, comprising both a sleep drive and a wake drive. Med. Hypotheses *60*, 509–512.

Edgar, D.M., and Seidel, W.F. (1997). Modafinil induces wakefulness without intensifying motor activity or subsequent rebound hypersomnolence in the rat. J. Pharmacol. Exp. Ther. *283*, 757–769.

Flores, A.E., Flores, J.E., Deshpande, H., Picazo, J.A., Xie, X.S., Franken, P., Heller, H.C., Grahn, D.A., and O'Hara, B.F. (2007). Pattern recognition of sleep in rodents using piezoelectric signals generated by gross body movements. IEEE Trans. Biomed. Eng. *54*, 225–233.

Forrest, D., Yuzaki, M., Soares, H.D., Ng, L., Luk, D.C., Sheng, M., Stewart, C.L., Morgan, J.I., Connor, J.A., and Curran, T. (1994). Targeted disruption of NMDA receptor 1 gene abolishes NMDA response and results in neonatal death. Neuron *13*, 325–338.

Fu, Y., Sander, J.D., Reyon, D., Cascio, V.M., and Joung, J.K. (2014). Improving CRISPR-Cas nuclease specificity using truncated guide RNAs. Nat. Biotechnol. *32*, 279–284.

Fujii, W., Kawasaki, K., Sugiura, K., and Naito, K. (2013). Efficient generation of large-scale genome-modified mice using gRNA and CAS9 endonuclease. Nucleic Acids Res. *41*, e187.

Glaab, T., Taube, C., Braun, A., and Mitzner, W. (2007). Invasive and noninvasive methods for studying pulmonary function in mice. Respir. Res. *8*, 63.

Gordon, C.J., and Ali, J.S. (1984). Measurement of ventilatory frequency in unrestrained rodents using microwave radiation. Respir. Physiol. *56*, 73–79.

Henson, M.A., Roberts, A.C., Pérez-Otaño, I., and Philpot, B.D. (2010). Influence of the NR3A subunit on NMDA receptor functions. Prog. Neurobiol. *91*, 23–37.

Hernandez, A.B., Kirkness, J.P., Smith, P.L., Schneider, H., Polotsky, M., Richardson, R.A., Hernandez, W.C., and Schwartz, A.R. (2012). Novel whole body plethysmography system for the continuous characterization of sleep and breathing in a mouse. J. Appl. Physiol. (1985) *112*, 671–680.

Horvath, P., and Barrangou, R. (2010). CRISPR/Cas, the immune system of bacteria and archaea. Science *327*, 167–170.

Hsu, P.D., Lander, E.S., and Zhang, F. (2014). Development and applications of CRISPR-Cas9 for genome engineering. Cell *157*, 1262–1278.

Kitano, H. (2002a). Computational systems biology. Nature *420*, 206–210.

Kitano, H. (2002b). Systems biology: a brief overview. Science *295*, 1662–1664.

Koek, W., Woods, J.H., and Winger, G.D. (1988). MK-801, a proposed noncompetitive antagonist of excitatory amino acid neurotransmission, produces phencyclidine-like behavioral effects in pigeons, rats and rhesus monkeys. J. Pharmacol. Exp. Ther. *245*, 969–974.

Laposky, A., Easton, A., Dugovic, C., Walisser, J., Bradfield, C., and Turek, F. (2005). Deletion of the mammalian circadian clock gene BMAL1/Mop3 alters baseline sleep architecture and the response to sleep deprivation. Sleep *28*, 395–409.

Li, Y., Erzurumlu, R.S., Chen, C., Jhaveri, S., and Tonegawa, S. (1994). Whisker-related neuronal patterns fail to develop in the trigeminal brainstem nuclei of NMDAR1 knockout mice. Cell *76*, 427–437.

Li, N., Lee, B., Liu, R.-J., Banasr, M., Dwyer, J.M., Iwata, M., Li, X.-Y., Aghajanian, G., and Duman, R.S. (2010). mTOR-dependent synapse formation underlies the rapid antidepressant effects of NMDA antagonists. Science *329*, 959–964.

Ma, M., Ye, A.Y., Zheng, W., and Kong, L. (2013). A guide RNA sequence design platform for the CRISPR/Cas9 system for model organism genomes. BioMed Res. Int. *2013*, 270805.

McShane, B.B., Galante, R.J., Biber, M., Jensen, S.T., Wyner, A.J., and Pack, A.I. (2012). Assessing REM sleep in mice using video data. Sleep *35*, 433–442.

Moghaddam, B., and Javitt, D. (2012). From revolution to evolution: the glutamate hypothesis of schizophrenia and its implication for treatment. Neuropsychopharmacology *37*, 4–15.

Mohamad, O., Song, M., Wei, L., and Yu, S.P. (2013). Regulatory roles of the NMDA receptor GluN3A subunit in locomotion, pain perception and cognitive functions in adult mice. J. Physiol. *591*, 149–168.

Mohn, A.R., Gainetdinov, R.R., Caron, M.G., and Koller, B.H. (1999). Mice with reduced NMDA receptor expression display behaviors related to schizophrenia. Cell *98*, 427–436.

Nagy, A. (2003). Manipulating the Mouse Embryo: A Laboratory Manual, Third Edition (Cold Spring Harbor, NY: Cold Spring Harbor Laboratory Press).

Radulovacki, M., Sreckovic, G., Zak, R., and Zahrebelski, G. (1984). Diazepam and midazolam increase light slow-wave sleep (SWS1) and decrease wakefulness in rats. Brain Res. *303*, 194–196.

Ran, F.A., Hsu, P.D., Wright, J., Agarwala, V., Scott, D.A., and Zhang, F. (2013). Genome engineering using the CRISPR-Cas9 system. Nat. Protoc. *8*, 2281–2308.

Sasaki, Y.F., Rothe, T., Premkumar, L.S., Das, S., Cui, J., Talantova, M.V., Wong, H.K., Gong, X., Chan, S.F., Zhang, D., et al. (2002). Characterization and comparison of the NR3A subunit of the NMDA receptor in recombinant systems and primary cortical neurons. J. Neurophysiol. *87*, 2052–2063.

Shi, M., Yue, Z., Kuryatov, A., Lindstrom, J.M., and Sehgal, A. (2014). Identification of Redeye, a new sleep-regulating protein whose expression is modulated by sleep amount. eLife *3*, e01473.

Shimba, S., Ogawa, T., Hitosugi, S., Ichihashi, Y., Nakadaira, Y., Kobayashi, M., Tezuka, M., Kosuge, Y., Ishige, K., Ito, Y., et al. (2011). Deficient of a clock gene, brain and muscle Arnt-like protein-1 (BMAL1), induces dyslipidemia and ectopic fat formation. PLoS ONE *6*, e25231.

Shiromani, P.J., Xu, M., Winston, E.M., Shiromani, S.N., Gerashchenko, D., and Weaver, D.R. (2004). Sleep rhythmicity and homeostasis in mice with targeted disruption of mPeriod genes. Am. J. Physiol. Regul. Integr. Comp. Physiol. *287*, R47–R57.

Snyder, E.M., Nong, Y., Almeida, C.G., Paul, S., Moran, T., Choi, E.Y., Nairn, A.C., Salter, M.W., Lombroso, P.J., Gouras, G.K., and Greengard, P. (2005). Regulation of NMDA receptor trafficking by amyloid-beta. Nat. Neurosci. *8*, 1051–1058.

Sumiyama, K., Kawakami, K., and Yagita, K. (2010). A simple and highly efficient transgenesis method in mice with the Tol2 transposon system and cytoplasmic microinjection. Genomics *95*, 306–311.

Sunagawa, G.A., Sei, H., Shimba, S., Urade, Y., and Ueda, H.R. (2013). FASTER: an unsupervised fully automated sleep staging method for mice. Genes Cells *18*, 502–518.

Sung, Y.H., Baek, I.J., Kim, D.H., Jeon, J., Lee, J., Lee, K., Jeong, D., Kim, J.S., and Lee, H.W. (2013). Knockout mice created by TALEN-mediated gene targeting. Nat. Biotechnol. *31*, 23–24.

Tong, G., Takahashi, H., Tu, S., Shin, Y., Talantova, M., Zago, W., Xia, P., Nie, Z., Goetz, T., Zhang, D., et al. (2008). Modulation of NMDA receptor properties and synaptic transmission by the NR3A subunit in mouse hippocampal and cerebrocortical neurons. J. Neurophysiol. *99*, 122–132.

van der Horst, G.T., Muijtjens, M., Kobayashi, K., Takano, R., Kanno, S., Takao, M., de Wit, J., Verkerk, A., Eker, A.P., van Leenen, D., et al. (1999). Mammalian Cry1 and Cry2 are essential for maintenance of circadian rhythms. Nature *398*, 627–630.

Wang, H., Yang, H., Shivalila, C.S., Dawlaty, M.M., Cheng, A.W., Zhang, F., and Jaenisch, R. (2013). One-step generation of mice carrying mutations in multiple genes by CRISPR/Cas-mediated genome engineering. Cell *153*, 910–918.

Wiedenheft, B., Sternberg, S.H., and Doudna, J.A. (2012). RNA-guided genetic silencing systems in bacteria and archaea. Nature *482*, 331–338.

Wisor, J.P., O'Hara, B.F., Terao, A., Selby, C.P., Kilduff, T.S., Sancar, A., Edgar, D.M., and Franken, P. (2002). A role for cryptochromes in sleep regulation. BMC Neurosci. *3*, 20.

Zhou, J., Wang, J., Shen, B., Chen, L., Su, Y., Yang, J., Zhang, W., Tian, X., and Huang, X. (2014). Dual sgRNAs facilitate CRISPR/Cas9-mediated mouse genome targeting. FEBS J. *281*, 1717–1725.